

Elimusertib has Antitumor Activity in Preclinical Patient-Derived Pediatric Solid Tumor Models

Fabian F. Pusch^{1,2}, Heathcliff Dorado García^{1,2}, Robin Xu^{1,2}, Dennis Gürgen³, Yi Bei^{1,2}, Lotte Brückner^{1,2,4}, Claudia Röefzaad^{1,2}, Jennifer von Stebut^{1,2}, Victor Bardinet¹, Rocío Chamorro Gonzalez^{1,2}, Angelika Eggert², Johannes H. Schulte^{2,5}, Patrick Hundsdörfer^{2,6}, Georg Seifert², Kerstin Haase¹, Beat W. Schäfer⁷, Marco Wachtel⁷, Anja A. Kühl⁸, Michael V. Ortiz⁹, Antje M. Wengner¹⁰, Monika Scheer², and Anton G. Henssen^{1,2,4,11,12}



ABSTRACT

The small-molecule inhibitor of ataxia telangiectasia and Rad3-related protein (ATR), elimusertib, is currently being tested clinically in various cancer entities in adults and children. Its preclinical antitumor activity in pediatric malignancies, however, is largely unknown. We here assessed the preclinical activity of elimusertib in 38 cell lines and 32 patient-derived xenograft (PDX) models derived from common pediatric solid tumor entities. Detailed *in vitro* and *in vivo* molecular characterization of the treated models enabled the

evaluation of response biomarkers. Pronounced objective response rates were observed for elimusertib monotherapy in PDX, when treated with a regimen currently used in clinical trials. Strikingly, elimusertib showed stronger antitumor effects than some standard-of-care chemotherapies, particularly in alveolar rhabdomyosarcoma PDX. Thus, elimusertib has strong preclinical antitumor activity in pediatric solid tumor models, which may translate to clinically meaningful responses in patients.

Introduction

Pediatric cancers are rare but represent a leading cause of death in children (1). Currently, pediatric solid tumors are treated with a histology-specific and risk-stratified combination of surgery, radiotherapy, and chemotherapy. Despite steady improvements in the survival rate of childhood cancers over the last several decades (2), cures remain unacceptably low for many high-risk pediatric solid tumors. Even for those who are ultimately cured, the aggressive multi-modality approaches are frequently associated with severe long-term morbidities (3). As a result, there is an urgent need to

identify novel therapeutic approaches, which leverage specific tumor vulnerabilities.

Compared with adult cancers, which often demonstrate high numbers of mutations accumulated over a lifetime, pediatric tumors generally arise during developmental windows in a tissue-context-specific manner, often harboring only few mutational drivers and a low mutational burden (4). A common feature among pediatric solid tumors is the presence of fusion oncoproteins, which emerge as a result of chromosomal aberrations (5). In addition, intra- and extrachromosomal oncogene amplifications are frequent in certain pediatric solid tumors, such as in neuroblastoma, where *MYCN* amplifications, often occurring on eDNA, are a predictor for poor prognosis (6–10). Both gene amplifications and fusion oncoproteins are hard to therapeutically target directly, particularly when affecting transcription factors, which has hampered the development of selective therapies in these tumor entities.

Genomic instability is a hallmark of cancer cells (11), which has recently been shown to be therapeutically actionable (12). The extreme proliferation rate in cancer cells, in part induced by fusion oncoproteins and oncogene amplifications, can result in delays or errors in the DNA termed replication stress (13–15). In response to the damaged DNA, cells have intricate mechanisms to recognize and repair lesions while ensuring that the cell cycle is halted, termed the DNA damage response (DDR). The DDR is mainly regulated by three kinases: Ataxia telangiectasia mutated (ATM), ataxia telangiectasia- and Rad3-related (ATR), and DNA-dependent protein kinase catalytic subunit (DNA-PKcs; ref. 16). Even though they have similar protein sequences, and their targets overlap, it is widely accepted that they respond to different stimuli (17). Although ATM and DNA-PKcs are mostly activated after double-strand breaks, ATR responds primarily to replication stress-associated DNA damage, which often involves single-stranded DNA intermediates (18, 19). Because ATR is activated in response to replication stress, it has been suggested that cancers depend on ATR more strongly than non-transformed cells to tolerate high levels of replication stress (20, 21). These findings have fueled the interest to test ATR inhibitors as a therapeutic option in cancer, particularly in tumors with high replication stress. Some biomarkers for predicting

¹Experimental and Clinical Research Center (ECRC) of the MDC and Charité Berlin, Berlin, Germany. ²Department of Pediatric Oncology and Hematology, Charité—Universitätsmedizin Berlin, Corporate Member of Freie Universität Berlin, Humboldt-Universität zu Berlin, Berlin, Germany. ³Experimental Pharmacology and Oncology (EPO), Berlin, Germany. ⁴Max-Delbrück-Centrum für Molekulare Medizin (BIMSB/BIH), Berlin, Germany. ⁵Department of Pediatric Oncology and Hematology, University Hospital Tübingen, Tübingen, Germany. ⁶Helios Klinikum Berlin-Buch, Berlin, Germany. ⁷University Children's Hospital, Zurich, Switzerland. ⁸IPATH.Berlin—Core Unit Immunopathology for Experimental Models, Charité Berlin, Corporate Member of Freie Universität Berlin, Humboldt-Universität zu Berlin, Berlin, Germany. ⁹Department of Pediatrics, Memorial Sloan Kettering Cancer Center, New York City, New York. ¹⁰Bayer AG, Berlin, Germany. ¹¹Berlin Institute of Health, Berlin, Germany. ¹²German Cancer Consortium (DKTK), partner site Berlin, and German Cancer Research Center (DKFZ), Heidelberg, Germany.

F.F. Pusch and H. Dorado García contributed equally as co-authors of this article.

Corresponding Author: Anton George Henssen, Charité—Universitätsmedizin Berlin, Berlin 13353, Germany. E-mail: anton.henssen@charite.de

Mol Cancer Ther 2024;23:507-19

doi: 10.1158/1535-7163.MCT-23-0094

This open access article is distributed under the Creative Commons Attribution-NonCommercial-NoDerivatives 4.0 International (CC BY-NC-ND 4.0) license.

©2023 The Authors; Published by the American Association for Cancer Research

ATR inhibitor response have been put forward, for example, ATM loss, TP53 loss, MYC overexpression, CDC25A overexpression, PGBD5 expression, and fusion oncoproteins such as EWS–FLI1 and PAX3–FOXO1, which increase sensitivity to ATR inhibitors (22–30) and are currently considered in clinical trial design (NCT04095273, NCT03188965, NCT03682289, NCT04170153, NCT04576091, NCT04535401, NCT04657068, NCT05338346, NCT04616534, NCT04514497, and NCT05071209). How most pediatric solid tumor entities may benefit from ATR inhibitor treatment is difficult to predict, as detailed preclinical information is currently missing.

Here, we profiled the antitumor effects of the ATR inhibitor elimusertib (also known as BAY 1895344; refs. 31, 32) *in vitro* and in a cohort of patient-derived xenografts (PDX) from pediatric solid tumors. To create a solid basis for future clinical trial designs, we compared the effects of elimusertib with those of first-line standard-of-care (SoC) chemotherapeutics. We demonstrate that monotherapy with elimusertib has most pronounced antiproliferative effects in models of alveolar rhabdomyosarcoma and neuroblastoma, and identify specific molecular alterations that may predict response to elimusertib. These findings highlight a potential therapeutic role for ATR inhibition in a subset of childhood solid tumors and provide a basis to accelerate the translation into meaningful clinical applications.

Materials and Methods

Study design

The purpose of this study was to examine the effects of ATR inhibition in preclinical models of pediatric solid tumors and identify potential biomarkers to select patients that could benefit from a treatment with the ATR inhibitor elimusertib. We first determined the inhibitory activity of the elimusertib in cell models, and compared these cells based on known determinants of ATR inhibition sensitivity, as well as the presence of oncogenes that increase the level of replication stress. We analyzed the effects of elimusertib treatment on cell-cycle control and genomic instability. All *in vitro* experiments were performed following the guidelines proposed by Arndt (33) for pediatric tumors. In the study, five to eight cell lines were used per disease, for which we validated the expression of the target genes and included the elimusertib IC₅₀ value after 72 hours. Outliers were not excluded unless technical errors were present. For *in vivo* testing, sample size was decided on the basis of previous experience with the models. Animals euthanized before the end of the experiment, due to excessive tumor growth or loss of body weight, were included in the analysis.

Reagents

All reagents were obtained from Carl Roth (Karlsruhe, Germany) unless otherwise indicated. Elimusertib (BAY1895344, 2-[(3R)-3-methylmorpholin-4-yl]-4-(1-methyl-1H-pyrazol-5-yl)-8-(1H-pyrazol-5-yl)-1,7-naphthyridine) was synthesized and provided to us by Bayer AG (Leverkusen, Germany). Its structure and synthesis have been previously published (31, 32). Elimusertib was dissolved in DMSO and stored at 10 mmol/L concentrations at –20°C until further use.

Cell culture

All neuroblastoma and Ewing sarcoma cell lines were kindly provided by Prof. J.H. Schulte (Charité). Rh41, Kym1, and Rh18 cells were a kind gift from Prof. Simone Fulda (Kiel, Germany). The remaining human tumor cell lines were obtained from the ATCC. All rhabdomyosarcoma and all Ewing sarcoma cell lines, as well as RPE

and BJ cell lines were cultured in DMEM (Gibco, Thermo Fisher Scientific) supplemented with 10% FCS (Thermo Fisher Scientific) and penicillin/streptomycin (Gibco, Thermo Fisher Scientific). All neuroblastoma cell lines were cultured in RPMI-1640 (Gibco, Thermo Fisher Scientific) supplemented with 10% FCM and penicillin/streptomycin. Twice per week, cells were washed with PBS, incubated in 0.05% Trypsin-EDTA (1x; Gibco, Thermo Fisher Scientific) for five minutes, resuspended in culture medium, sedimented at 500 × g for 5 minutes and a fraction was cultured in fresh media. Cells were kept in culture for a maximum of 30 passages. Resuspended cells were counted by mixing 1:1 with 0.02% trypan blue in a Bio-Rad TC20 cell counter. Cell line authenticity was confirmed by STR genotyping. The absence of *Mycoplasma sp.* contamination was determined using a Lonza MycoAlert system. All cell lines used are listed in Supplementary Table S1.

Cell viability

Cell viability was assessed using CellTiter-Glo (Promega). Briefly, for CellTiter-Glo measurement, 1,000 cells were seeded in white, flat-bottom, 96-well plates. After 24 hours, drugs were added to the medium and cells were incubated for 72 hours. CellTiter-Glo luminescent reagent was added according to the manufacturer's protocol, and the luminescence signal measured on a Glowmax-Multi Detection System (Promega).

Colony formation assays

Flat and transparent 24-well plates were incubated with 0.1% poly-D-lysine for 30 minutes, washed twice with PBS and then left open to dry under UV radiation for 30 minutes. Depending on the individual cell type and growth rate, 1,000–2,000 single cells have been plated in each well and were able to attach for 24 hours. Experiments were performed in triplicates with either 48 hours treatment of elimusertib at the cell lines corresponding IC₅₀ value or DMSO control. After 48 hours, the media were removed and the wells were carefully washed twice with cell culture medium and then cultured in drug-free media for 7–10 days. Resultant colonies were fixed with 1% PFA and stained with crystal violet.

Western immunoblotting

Whole-cell protein lysates were prepared by lysing cells in RIPA supplemented with cOmplete Protease inhibitor (Roche) and PhosphoStop (Roche). Protein concentrations were determined by bicinchoninic acid assay (Thermo Fisher Scientific). 10 µg of protein were denatured in Laemmli buffer at 95°C for 5 minutes. Lysates were loaded onto 16%, or 10% Tris-Glycine (Thermo Fisher Scientific) gels for gel electrophoresis depending on the protein sizes of interest. Proteins were transferred onto polyvinylidene difluoride membranes (Roche), blocked with 5% dry milk or 5% BSA for 1 hour and incubated with primary antibodies overnight at 4°C, then secondary antibodies for 1 hour at room temperature. Chemiluminescent signal was detected using Enhanced chemiluminescence (ECL) Western Blotting Substrate (Thermo Fisher Scientific) and a Fusion FX7 imaging system (Vilber Lourmat, Marne-la-Vallée, France). Quantification was performed with ImageJ.

Immunofluorescence staining

Cells were grown at the desired confluency on glass slides with an 8-well flexiPERM silicone grid (Sarstedt, 94.6032.039) for 24 hours and directly processed (for R-loop quantification) or treated with 20 nmol/L elimusertib for 48 hours (micronuclei quantification). Cells were washed with PBS three times and fixed for 10 minutes with 3.7% paraformaldehyde, washed with PBS three times and permeabilized

with PBS containing 0.1% Triton-X100. For R-loop immunofluorescence cells were blocked for 30 minutes with 10% FCS in PBS-T (0.2% Tween-20 in PBS), incubated overnight at 4°C with the primary antibody (Anti-DNA-RNA Hybrid Antibody, clone S9.6; Merck Millipore MABE1095), washed three times with PBS-T (0.05% Tween-20 in PBS), incubated for 1 hour in the dark at room temperature with the secondary antibody (Dianova, 715-096-150). After removal of the 8-well silicone grid, the glass slide was washed three times with PBS-T (both R-loop and micronuclei quantification). The glass slide was covered with DAPI-containing mounting media (Vectashield, Vec-H-1000) and mounted with a cover slip. Cells were imaged using an ECHO Revolve microscope and quantified using ImageJ.

FACS

Cells were grown in the presence of drug or vehicle (DMSO) for 72 hours before sample preparation for flow cytometry. For cell-cycle analysis, cells were incubated with 5-Ethynyl-2'-deoxyuridine (EdU) for 2 hours right before fixation and fluorescent labeling, following the instructions provided in the kit Click-IT EdU Alexa Fluor 488 Flow Cytometry Assay kit (Thermo Fisher Scientific). For DNA damage analysis, TUNEL was performed using the APO-BrdU TUNEL Assay Kit (Thermo Fisher Scientific), according to the manufacturer's descriptions. Stained cells were measured on a BD LSR Fortessa flow cytometer (BD Biosciences) and analyzed using FlowJo (v 10.8.1).

PDX treatment

The establishment of PDX models was conducted as previously described (34) in collaboration with Experimental Pharmacology & Oncology GmbH (EPO, Berlin, Germany), from patients accepted for treatment in Charité University Medicine. All experiments were conducted according to the institutional animal protocols and the national laws and regulations. Tumor fragments from patients were serially transplanted into either Crl:NMRI-Foxn1^{tmu} mice (Charles River Laboratories) or NOD.Cg-Prkdc^{scid} Il2rg^{tm1Sug}/JicTac mice (Taconic, Rensselaer, NY, USA) for the establishment of the PDX up to passage 3–9, when the experiment was performed. Tumor growth was monitored with caliper measurements. Tumor volume was calculated with the formula length × width²/2. PDX were serially transplanted in mice at least three times before the experiments. Mice were randomized into four groups with at least 3 mice to receive treatment. For the elimusertib study, mice were administered 40 mg/kg body weight on a 3 days-on/4 days-off regime twice daily (orally). Elimusertib was dissolved in 60% polyethylene glycol 400, 10% ethanol, and 30% water to a 4 mg/mL solution, the same solution without compound was used as vehicle control. Mice were sacrificed by cervical dislocation once the tumor volume exceeded 1,500 mm³ or body weight loss was higher than 20%.

The PDXs used in this study are available for the scientific community under a material transfer agreement with Experimental Pharmacology & Oncology GmbH (EPO, Berlin, Germany). Currently, 28 out of 32 PDXs are part of the international PDX repository ITCC-P4.

IHC stainings

Paraffin sections of 1-µm thickness were cut, dewaxed, and subjected to a heat-induced epitope retrieval step. Endogenous peroxidase was blocked by hydrogen peroxide before incubation with anti-Ki67 (clone D2H10, Cell Signaling Technology), anti-Histone H3-S10 (polyclonal rabbit, Abcam #47297) or anti-γH2AX (polyclonal rabbit, Abcam #229914) followed by incubation with EnVision+ horseradish peroxidase-labeled polymer (Agilent). For visualization, 3,3'-diaminobenzidine as chromogen was used. For detection of cleaved cas-

pase3, anti-clCasp3 (clone 5A1E, Cell Signaling Technology) was used followed by incubation with secondary antibody (biotinylated donkey anti-rabbit) and alkaline phosphatase-labeled streptavidin (Agilent). RED was used as chromogen (Agilent). Nuclei were stained with hematoxylin (Merck) and slides were coverslipped in glycerol gelatine (Merck). Multispectral images were acquired using a Vectra 3 imaging system (Akoya Biosciences). The QuPath software (version 0.3.2) was used for cell segmentation as well as quantification.

Cell line and PDX genomic analysis

Cell line mutation data were obtained from the online public dataset DepMap (<https://depmap.org/portal/>, packages Copy Number Public 21Q2 and Mutation Public 21Q2).

Whole-exome sequencing (WES) from the Sarcoma PDX samples was performed using the NEBNext Ultra II FS DNA library Kit for Illumina (New England BioLabs), SureSelectXT HS Target Enrichment System for Illumina Paired-End Multiplexed Sequencing Library for Illumina Multiplexed Sequencing Platforms (Agilent), and TruSeq Stranded mRNA Library Prep (New England BioLabs), respectively, following the protocol provided by the manufacturers. Sequenced reads were trimmed using TrimGalore (v0.6.4_dev) and aligned to a merged genome consisting of hs37d5 and mm10 using Burrows-Wheeler Aligner (BWA)-MEM (v.0.7.17). Duplicate reads were marked using UMI-tools (v.1.0.1). Base qualities were recalibrated using GATK4 suite (v4.1.4.1). Single-nucleotide variants were identified following the GATK4 Somatic short variant discovery (SNVs + Indels) best practice workflow by calling GATK4/Mutect2 (v.4.1.4.1) in tumor-only mode with allele frequencies from gnomAD's germline-resource. Candidate variants were further filtered following the workflow and variants were annotated using SnpEff (v4.3t) and SnpSift (v4.3t). Copy-number alterations were called following the CNV kit (0.9.10.dev0) copy-number calling pipeline. Relative copy-number (rCN) ratios were converted to ploidy adjusted absolute copy number (paCN) using following formula:

$$paCN = 2^{(rCN + \log_2(Ploidy))}$$

Ploidy values were derived from the PureCN (v.2.1.7) R package. Gains and losses are defined as paCN > log₂(3/2) and paCN < log₂(1/2), respectively.

Neuroblastoma PDX sequencing data and variant calls were downloaded from the IMI2 ITCC-P4 project (<https://www.itccp4.eu/>). Oncoplots were drawn using the R package maftools (v 2.12.0).

Statistical analysis

All statistical tests were done using GraphPrism9 or R.

Data availability

The data generated in this study are available upon request from the corresponding author. Restrictions apply to the availability of data that does not comply with patient privacy requirements. Sarcoma PDX WES reads have been deposited to the European Genome-phenome Archive (<https://www.ebi.ac.uk/ega/>) under accession number EGAS50000000048.

Ethics statement

The *in vivo* experiments were conducted in accordance with the German Animal Welfare Act and have been approved by an Institutional Animal Care and Use Committee with regards to national laws and regulations (Landesamt für Gesundheit und Soziales, LaGeSo Berlin, Germany).

Results

Elimusertib treatment affects survival of pediatric solid tumor cell lines

To study the therapeutic potential of elimusertib inhibition in pediatric solid tumors, we treated 36 cell lines derived from several pediatric tumors, including Ewing sarcoma (EWS), alveolar (ARMS), and embryonal rhabdomyosarcoma (ERMS) and high-risk neuroblastoma with and without *MYCN* amplification (MNA NB vs. NMNA NB), with the ATR inhibitor elimusertib and measured their survival over time (Fig. 1A–C; Supplementary Fig. S1A–S1Y). Cells showed a wide range of response, with inhibitory 50% concentrations (IC_{50}) values ranging from 2.687 to 395.7 nmol/L (Supplementary Table S1). These concentrations are well below plasma concentrations achievable in human patients (35), suggesting that elimusertib may exert similar anti-tumor effects *in vivo*. Compared with non-transformed cell lines BJ and RPE cells, elimusertib inhibited cell viability at lower concentrations in most cancer cell lines (Fig. 1D). In line with previous reports testing other ATR inhibitors (24, 26, 29), cell lines derived from Ewing sarcoma, *MYCN*-amplified neuroblastoma, and alveolar rhabdomyosarcoma were (significantly) more sensitive to ATR inhibition than control cell lines, suggesting that a therapeutic window may exist for elimusertib in these pediatric solid tumors.

In addition, we performed colony formation assays in a subset of pediatric cancer cells that showed a reduced ability of survival and proliferation in the elimusertib-treated group versus DMSO control (Fig. 1E and F).

Elimusertib treatment leads to DNA damage in pediatric solid tumor cell lines

ATR is a key regulator of replication stress-induced DNA damage (18, 36, 37). To investigate the effects of ATR inhibition in pediatric cancer cell lines, we measured DNA damage accumulation in response to elimusertib treatment in a subset of cell lines. Micronucleation is an indicator of genomic instability (38). In response to elimusertib, cell lines showed higher rates of micronucleation (Fig. 1G and H), indicating the presence of DNA damage. Co-staining with TUNEL and propidium iodide indicated an increase in the fraction of cells with fragmented DNA in cells incubated with elimusertib, suggesting an accumulation of unrepaired damaged DNA and apoptotic DNA fragmentation (Fig. 1I and J), which is in line with previous reports (26, 29, 31, 35, 39). Furthermore, we observed an increase of sub- G_1 fragments upon treatment with elimusertib, emphasizing the ability to induce cell death in treated cells (Supplementary Fig. S2A and S2B). Because ATR is crucial for the intra-S and G_2 -M checkpoint activation (40–42), we examined cell-cycle progression in response to elimusertib. We pulse-labeled replicating DNA with 5-EdU and stained all DNA with propidium iodide in cells incubated in the presence of elimusertib. In all cell lines tested, elimusertib led to a reduction in the fraction of cells in S-phase, consistent with a repression of the intra-S checkpoint. In all cell lines but one (IMR-5/75), we observed an increase in cells in G_2 -M (Fig. 1K and L). To assess whether cells accumulated in mitosis, consistent with a G_2 -M checkpoint suppression, we measured Histone 3 phosphorylation at Serine 10, a marker specific for mitosis (43). After incubation in the presence of elimusertib, we did not observe a consistent increase in IMR-5/75 (neuroblastoma) and TC-253 (Ewing sarcoma) cells, suggesting cell context dependent cell-cycle

disruption in response to elimusertib (Supplementary Fig. S3A and S3B). We next evaluated the effect of elimusertib on replication stress by measuring RPA32 T21 phosphorylation, in cells incubated with elimusertib. RPA32 phosphorylation, a marker of single-stranded DNA, was increased in response to elimusertib (Supplementary Fig. S3A and S3B). Taken together, this suggests that elimusertib prevents repair of replication stress-associated DNA damage, resulting in further genomic instability and then ultimately apoptosis in these pediatric solid tumor cell line models.

Fusion oncoprotein expression and high *MYCN* levels are associated with elimusertib sensitivity

Because ATR is key in repairing replication stress-induced DNA damage, we tested whether cell lines with varying levels of ATR-mediated replication stress response signaling would differ in their sensitivity to elimusertib. For this purpose, we assessed the abundance of R-loops, a nucleic acid structure consisting of an RNA:DNA hybrid and single-stranded DNA that has been implicated in genomic instability as well as replication stress and is being discussed as mediator for treatment susceptibility in cancer (44, 45). In contrast with previous reports, no positive correlation was observed between the abundance of R-loops and elimusertib sensitivity (Supplementary Fig. S4A–S4C). Sensitivity to ATR inhibitors can be influenced by genetic aberrations frequent in cancers, such as TP53 or ATM loss, PGBD5, *MYC(N)* expression, or fusion oncoproteins such as EWS-FLI1 and PAX3-FOXO1 (22, 24–27, 29, 46). We assessed the presence of frequent genetic alterations in pediatric tumors (47) as well as markers that cause genetic vulnerability to ATR inhibition (22, 25, 27, 28, 48, 49) in our cell lines using publicly available datasets (50). In line with previous reports (28), the presence of *MYCN* amplifications, both on ecDNA or as homogeneously staining regions (51, 52), in NB cell lines, expression of fusion oncoproteins such as EWS-FLI1 or PAX3-FOXO1 (25, 29), and TP53 deficiency (22) were associated with higher elimusertib sensitivity (Fig. 1M). Thus, the presence of known biomarkers of ATR inhibitor sensitivity is also associated with elimusertib sensitivity in pediatric tumor cell lines and may be suitable for patient selection in current and upcoming clinical trials.

A preclinical trial of elimusertib in PDXs demonstrates clinically relevant response in a large subset of pediatric solid tumors

Encouraged by the results obtained *in vitro*, we sought to test the preclinical antitumor activity of elimusertib *in vivo* in mice harboring PDX models of pediatric solid tumors (Fig. 2A). We selected a cohort of PDX derived from 8 Ewing sarcomas, 4 ERMS, 7 ARMS, 4 MNA-NB, 5 NMNA-NB, 3 osteosarcomas, and one CIC-DUX fusion gene expressing undifferentiated sarcoma. Within each entity, the cohort comprised various sites of origin, primary or relapse status, histopathological gradings and clinical stagings (Supplementary Table S2). In total, we treated 195 mice (median 3 mice per PDX model and treatment arm) and 32 PDX models derived from patients treated at the Charité – Universitätsmedizin Berlin and the University Children's Hospital, Zurich (53). Some PDXs were derived from the same tumors but collected before and after treatment (EWS_3a and EWS_3b) or sequential relapses (ERMS_2a, ERMS_2b and ERMS_2c; Supplementary Table S2). To closely mirror the setup of a clinical trial, we treated mice using the same regimen currently used in clinical trials, for example, elimusertib at 40 mg/kg body weight twice daily per oral gavage, on a 3 days-on/4 days-off schedule for 28 days (Fig. 2A). According to the RECIST (54, 55), two of the PDX models achieved a complete response (CR), two PDX had a partial response (PR), 14 PDX

Elimusertib has Antitumor Activity in Pediatric Solid Tumors

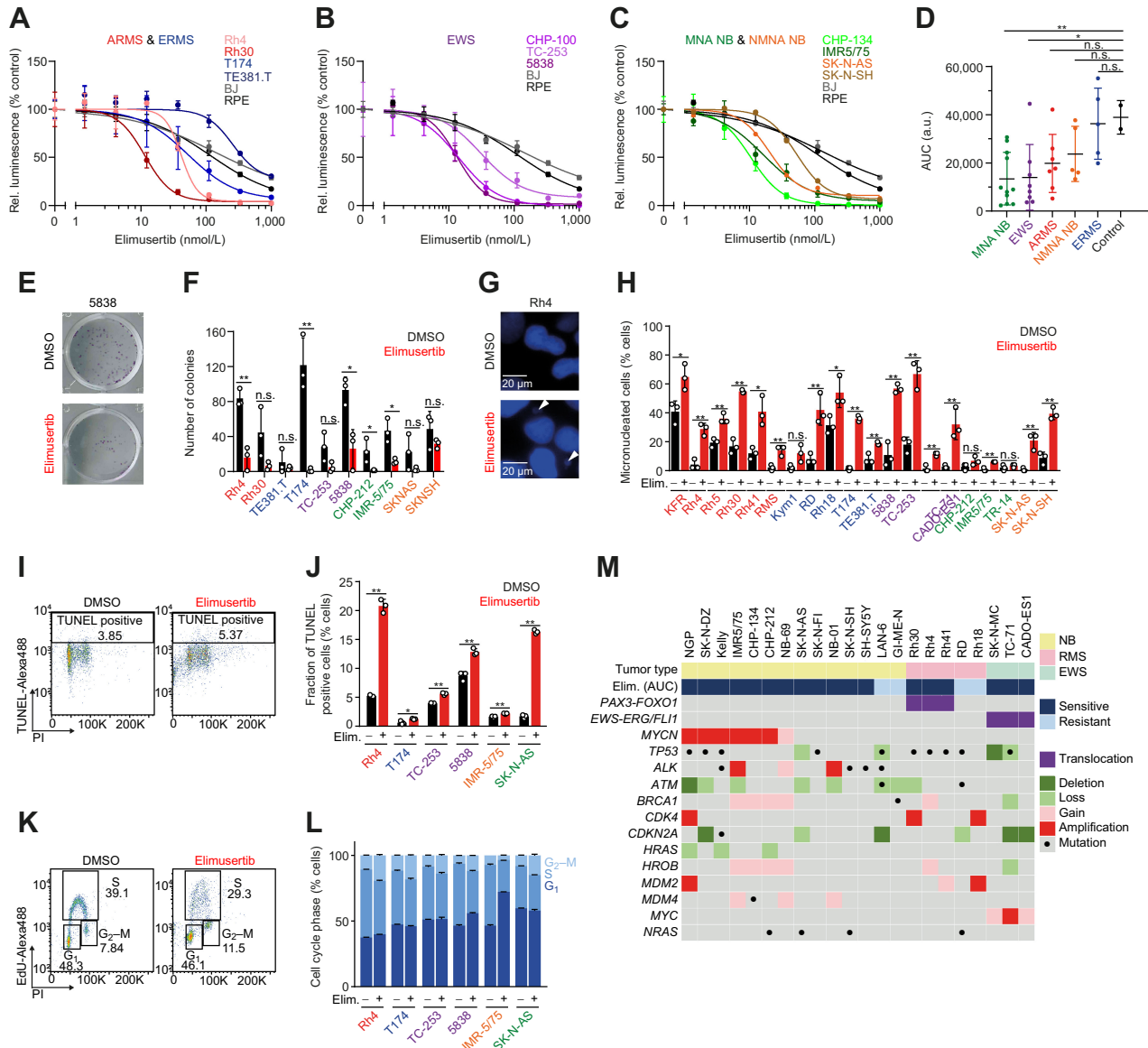
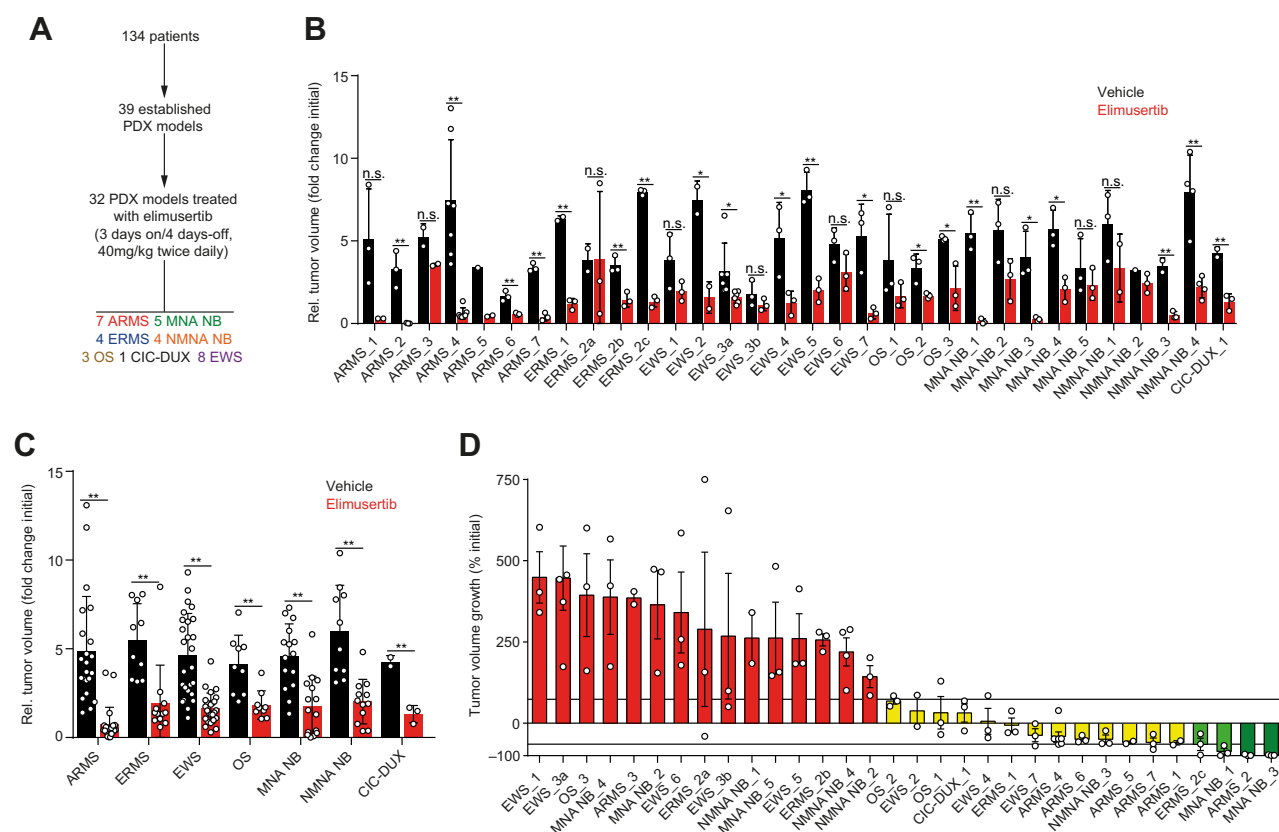


Figure 1.

Elimusertib shows antitumor activity in a broad spectrum of pediatric cancer cell lines. **A-C**, Dose-response curves of the cell viability for ARMS (**A**), ERMS (**A**), Ewing sarcoma (**B**), MNA NB (**C**), and NMNA NB cell lines (**C**) treated with the ATR inhibitor elimusertib compared with non-cancer cell lines BJ and RPE ($n = 3$; 50% inhibitory concentrations, IC_{50} , and area under the curve, AUC, values are listed in Supplementary Table S1). **D**, AUC corresponding to the graphs in (**A-C**; unpaired, two-sided Student t test, $P = 0.0096, 0.0410, 0.0761, 0.1488, 0.8260$ for MNA NB vs. Control, Ewing sarcoma vs. Control, ARMS vs. Control, NMNA_NB vs. Control, ERMS vs. Control, respectively). **E**, Representative pictures of a colony formation assay in 5,838 cells treated at corresponding IC_{50} value for 48 hours and cultivated for 7–10 days ($P = 0.0022, 0.0821, 0.4753, 0.0028, 0.0786, 0.0121, 0.0466, 0.0124, 0.1685, 0.2402$, respectively; $n = 3$). **G**, Representative photomicrographs of micronuclei (white arrow) in cells treated with elimusertib. **H**, Fraction of micronucleated cells after treatment with elimusertib (20 nmol/L) for 72 hours ($P = 0.0242, 0.0014, 0.0033, 0.0002, 0.0108, 0.0065, 0.520, 0.0061, 0.0312, 1.30 \times 10^{-5}, 0.0072, 0.0008, 0.0014, 0.0026, 0.0088, 0.1448, 0.0013, 0.3740, 0.0030, 0.0042, 0.0008, 0.0008$, respectively; $n = 3$, with 50 cells per replicate). **I**, Representative gating for TUNEL labeling in 5,838 cells. **J**, Quantification of TUNEL signal in a set of pediatric solid tumor cell lines treated with elimusertib (20 nmol/L) for 72 hours. ($P = 2.08 \times 10^{-5}, 0.0232, 0.0002, 0.0018, 0.0045, 6.38 \times 10^{-7}$, respectively; $n = 3$). **K**, Representative gating for EdU and PI co-staining in 5,838 cells. **L**, Quantification of the fraction of cells in each cell-cycle phase in a set of pediatric solid tumor cell lines after elimusertib treatment (20 nmol/L) for 72 hours ($n = 3$; error bars represent standard deviation). **M**, Table of mutations (including translocations, single-nucleotide variants, and copy-number alterations) affecting genes associated with ATR inhibitor sensitivity in a subset of cell lines tested. * t test resulting in $P < 0.05$; ** t test resulting in $P < 0.01$.

**Figure 2.**

Elimusertib treatment induces heterogeneous response in a large cohort of patient-derived xenografts of pediatric solid tumors. **A**, Schematic representation of the preclinical study in PDX models. A total of 39 PDX models were established from 134 patients. 32 of those PDXs received 40 mg/kg body weight elimusertib twice daily per oral gavage, on a 3 days-on/4 days-off schedule. **B**, Dot plot showing the relative tumor volume at the end of the treatment for all PDXs treated with elimusertib or vehicle control (n and P values are listed in Supplementary Table S3). **C**, Dot plot showing the relative tumor volume at the end of the treatment for all tumor entities treated with elimusertib or vehicle control (n and P values are listed in Supplementary Table S3). **D**, Waterfall plot representing tumor volume change in mice receiving elimusertib. Tumors were classified according to the RECIST criteria (55) as progressive disease (red), stable disease (yellow), partial response (light green), and complete response (dark green). For statistical comparison, an unpaired, two-sided Student t test was performed; error bars represent standard deviation. * $P < 0.05$; ** $P < 0.01$.

were considered as stable disease (SD), and 16 PDX were classified as progressive disease (PD, Fig. 2B–D; Supplementary Table S3). In all cases, single-agent elimusertib treatment was sufficient to significantly delay tumor growth, compared with vehicle-treated control mice (Supplementary Fig. S5A–S5AF). Consistent with our previous work using AZD6738 (29) mice harboring PDX derived from ARMS showed the most pronounced response, with only one out of the seven ARMS PDX models classified as PD after elimusertib treatment (Supplementary Fig. S5A–S5G). ERMS (Supplementary Fig. S5H–S5K) and MNA NB PDX (Supplementary Fig. S5W–S5AA) also showed a good response, with only one and two models demonstrating a PD, respectively. Interestingly, the ERMS model derived from the same patient showed a better response than the models derived from the same patient at an earlier time point (ERMS_2a and ERMS_2b, respectively; Fig. 2B and C; Supplementary Fig. S5I–S5K), implicating that treatment-associated tumor evolution may have enhanced ATR inhibitor sensitivity. Toxicity, assessed by body weight loss over time, was minimal during treatment, indicating a good tolerability of the drug in the given regimen (Supplementary Fig. S6A–S6AF). Together, elimusertib monotherapy has clinically relevant antitumor activity in pediatric solid tumor models.

Elimusertib treatment extends progression-free survival in pediatric solid tumor models

To further evaluate the preclinical activity of elimusertib, we assessed the progression-free survival (PFS) of PDX after elimusertib treatment. Overall, elimusertib extended the median PFS from 7 to 20 days across PDX models from different tumor entities (Fig. 3A). The most pronounced extension of PFS was observed for ARMS (Fig. 3B, median PFS from 9 days to the end of experiment), followed by ERMS (Fig. 3C, median PFS from 5 to 26 days). Median PFS increased from 7 to 14 days for Ewing sarcoma (Fig. 3D), from 6 to 12 days for MNA NB (Fig. 3E), 7 days to 17 for NMNA NB (Fig. 3F), 9 to 20 days for osteosarcoma (Fig. 3G), and 5 to 12 days for the CIC-DUX model (Fig. 3H). Furthermore, elimusertib prolonged overall survival across PDX from all tumor entities with a median overall survival of 19 versus 31 days in the untreated and elimusertib-treated groups, respectively (Supplementary Fig. S7A). For some tumor entities, such as ARMS, ERMS, NMNA NB, and osteosarcoma, the overall survival rate in the treatment group was significantly higher than the control group at 30 days, exceeding 75% overall survival (Supplementary Fig. S7B, S7C, S7F, and S7G). MNA NB and Ewing sarcoma also showed significantly prolonged overall survival, whereas

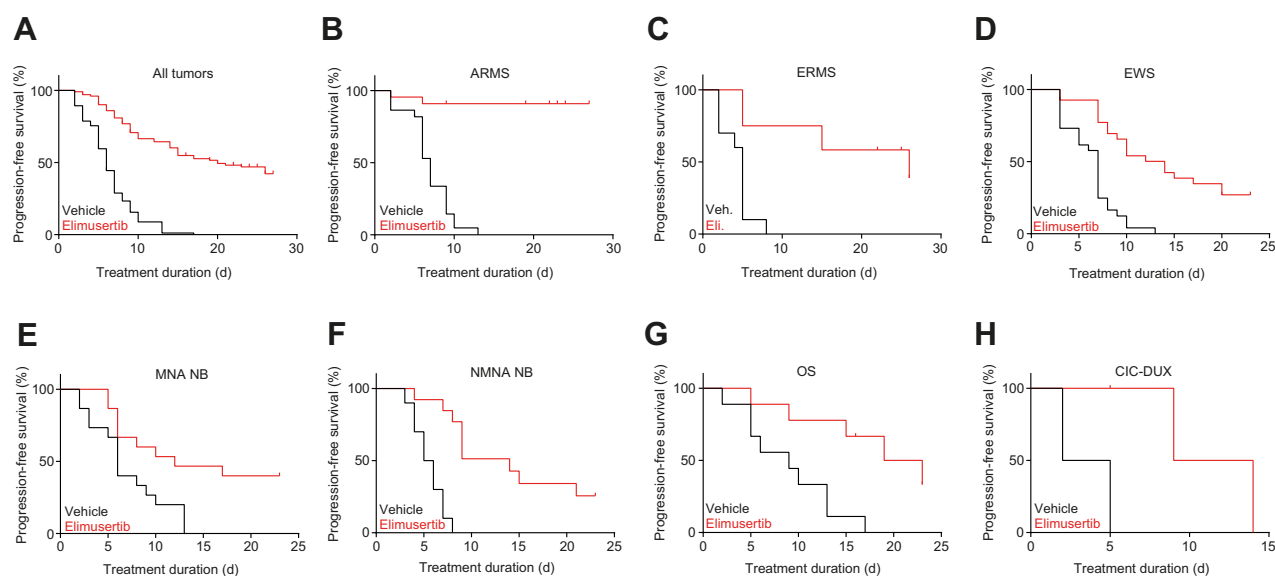


Figure 3.

Elimusertib treatment extends the progression-free survival of preclinical pediatric solid tumor models. **A–H**, Kaplan-Meier curves showing the progression-free survival, defined as time until the tumor was classified as progressive disease, PD, according to the RECIST criteria, in mice treated with elimusertib (red) or vehicle (black), across tumor types (**A**, $n_{total} = 195$, $P < 0.0001$), ARMS (**B**, $n_{total} = 44$, $P < 0.0001$), ERMS (**C**, $n_{total} = 22$, $P = 0.0001$), Ewing sarcoma (**D**, $n_{total} = 53$, $P < 0.0001$), MNA NB (**E**, $n_{total} = 30$, $P = 0.0064$), NMNA NB (**F**, $n_{total} = 23$, $P < 0.0001$), osteosarcoma (**G**, $n_{total} = 18$, $P = 0.0033$) and CIC-DUX sarcoma (**H**, $n_{total} = 5$, $P = 0.0389$). Log-rank tests were performed for statistical comparison.

the overall survival of the CIC-DUX models was not statistically significant (Supplementary Fig. S7D, S7E, and S7H). Thus, elimusertib monotherapy delays tumor growth, which results in pronounced increases in PFS and overall survival in diverse pediatric solid tumor models.

Elimusertib leads to reduced proliferation in pediatric solid tumor PDX

To characterize the effect of elimusertib treatment on PDX, we performed IHC staining of molecular markers of cell proliferation, DNA damage and apoptosis in 21 of the 32 PDX models at the end of elimusertib treatment (Supplementary Figs. S8–S12; Supplementary Tables S4–S6). Baseline expression of these markers was not associated with differences in elimusertib response (Supplementary Fig. S13A, S13C, and S13D). Only high pre-treatment Histone H3 phosphorylation (pHH3) expression, indicative of mitotic cells, was slightly associated (not statistically significant) with good PDX response (Supplementary Fig. S13B). The fraction of Ki-67-positive cells, an indicator of proliferating cells, in PDX was significantly lower in elimusertib- than vehicle-treated PDX (Fig. 4A and B), in line with the reduced cell proliferation observed after elimusertib treatment *in vitro* (Fig. 1). Notably, favorable response to elimusertib treatment, as defined using the RECIST criteria, was associated with low fractions of Ki-67-expressing cells after treatment (overall responding PDX, OR, composed of SD, PR and CR, Fig. 4C). In contrast, in poorly responding PDX, that is, with PD, differences in Ki-67 staining after elimusertib treatment were not significant (Fig. 4D–I). Similarly, Histone H3 phosphorylation, a marker of mitosis, was lower after elimusertib treatment in 8 out of 9 PDXs classified as responsive (OR, Supplementary Fig. S12A–S12H). Thus, reduced cell proliferation is more pronounced in PDXs responsive to elimusertib. In addition, PDXs were stained for histone variant γ H2A.X Ser139 phosphorylation (γ H2AX), a marker of DNA damage, and cleaved caspase-3

(Clc3), a marker of apoptosis. In contrast with our *in vitro* results, no significant differences in H2A.X Ser139 phosphorylation or caspase-3 cleavage were observed in PDXs treated with elimusertib compared with vehicle-treated PDXs (Supplementary Fig. S12I–S12X). This may be because DNA damage induction and apoptosis precede reduced cell proliferation in tumors, hence was not detectable at the end of the treatment period. Thus, elimusertib leads to reduced Ki-67 expression, indicative of altered tumor cell proliferation, which also positively correlated with tumor response *in vivo*.

Elimusertib shows stronger antitumor effects than some SoC treatment regimens in a subset of preclinical pediatric solid tumor models

Pediatric solid tumors are currently treated with a combination of chemotherapeutic agents. To evaluate the clinical potential of elimusertib, we aimed to compare the antitumor effects of elimusertib in our cohort of PDXs with the effects of current SoC agents. Despite minor differences in exact composition, most pediatric tumors in Europe and the United States are treated in the first line with a combination of topoisomerase inhibitors, mitotic inhibitors, antimetabolites, intercalating, and alkylating agents (56–59). The response to the abovementioned chemotherapeutic agents was evaluated using modified RECIST criteria. We here compared the responses with the SoC chemotherapeutics with the response to elimusertib (Fig. 5A). Notably, most PDXs were relatively unresponsive to SoC chemotherapeutics as monotherapy, which was not associated with prior exposure to these treatments in patients from which PDX were derived. Intriguingly, some of the PDXs that were relatively chemo-resistant responded well to elimusertib, indicating that patients that develop resistance to current SoC treatments may still benefit from elimusertib treatment (Fig. 5). We next compared the changes in PFS following elimusertib treatment with that of SoC chemotherapeutic agents (Fig. 5B–F). Strikingly, elimusertib prolonged the PFS of all ARMS

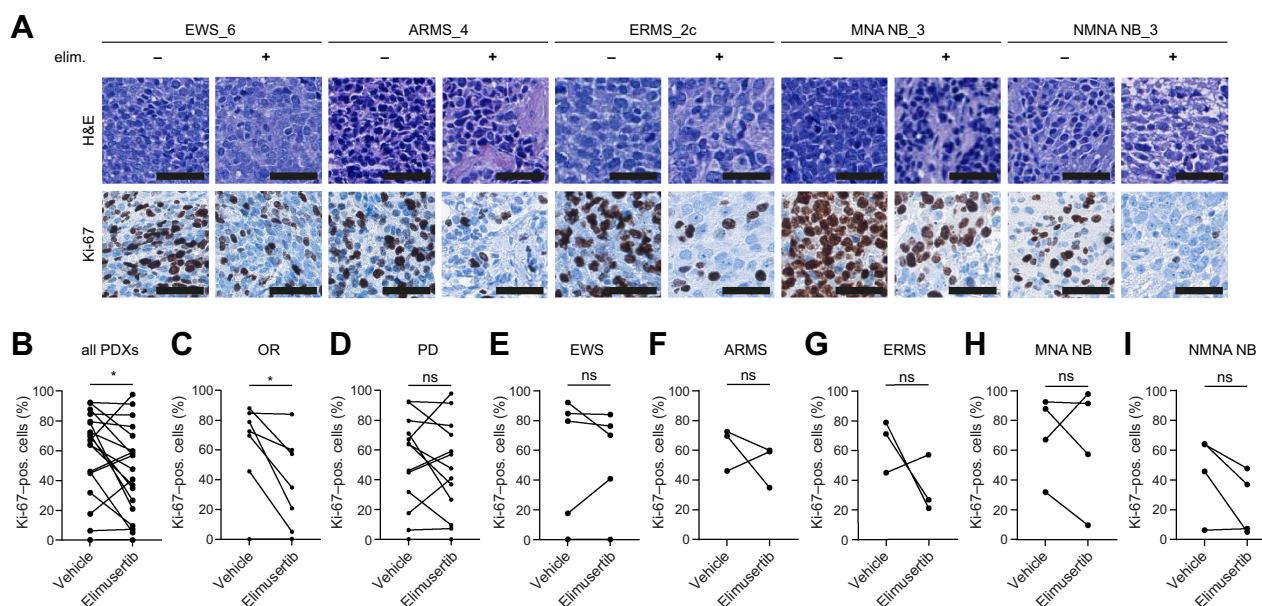


Figure 4.

Elimusertib reduces the proliferation rate in PDX models of pediatric solid tumors. **A**, Exemplary hematoxylin and eosin and Ki-67 stainings of Ewing sarcoma, ARMS, ERMS, MNA NB, and NMNA NB PDXs treated with elimusertib or vehicle control. **B–I**, changes in the fraction of Ki-67-expressing cells for all PDXs combined (**B**), PDXs responding to elimusertib as defined per RECIST (OR, **C**) and PDXs with progressive disease (PD, **D**), Ewing sarcoma (**E**), ARMS (**F**), ERMS (**G**), MNA NB (**H**), and NMNA NB (**I**). ($n = 10$; paired, two-sided Student t test; error bars represent standard deviation, $P = 0.0371, 0.0216, 0.4764, 0.9394, 0.4935, 0.2945, 0.7005$, and 0.0933 for all PDXs combined, responding PDXs, PDXs with progressive disease, Ewing sarcoma, ARMS, ERMS, MNA NB, and NMNA NB, respectively); scale bar, $40 \mu\text{m}$.

and NMNA NB PDX to a greater extent than any of the SoC agents (Fig. 5B and F; Supplementary Table S7). A similarly pronounced prolonged PFS advantage was observed compared with most chemotherapeutic agents tested in ERMS and MNA NB PDX (Fig. 5C and E; Supplementary Table S7). Only Ewing sarcoma PDX responded similarly to elimusertib as they did to chemotherapy (Fig. 5D; Supplementary Table S7). Thus, our in-depth preclinical response evaluation suggests that elimusertib could have clinically relevant antitumor effects in many pediatric tumor entities and may in some cases be superior to currently used treatment options.

SoC treatment-associated genomic evolution reveals candidate alterations that render PDXs susceptible to ATR inhibition

As shown *in vitro* (Fig. 1M) and suggested by previous reports (22–28, 30), distinct molecular alterations may predict good response to ATR inhibitors. We genetically characterized a subset of the PDX models using WES. None of the genetic alterations identified in our cohort were associated with therapy response across all or within different entities (Fig. 6A–F). Thus, we focused our analysis on genetic alterations in otherwise near-isogenic PDX pairs derived from the same patients with particularly strong elimusertib response differences (Fig. 6G and H). For example, three ERMS PDX (ERMS_2a–c) derived from subsequent relapses responded very differently to elimusertib, with the best response observed in the PDX derived from the latest relapse (ERMS_2c, Fig. 6B; Supplementary Fig. S5I–S5K). Intriguingly, mutations in *BRCA1* and *FGFR4* were only detected in the responsive PDX (ERMS_2c) and not in the two PDX derived from earlier clinical time points (ERMS_2a+b), suggesting that these mutations occurred later during patient treatment. *BRCA1* deficiency has been implicated in ATR inhibitor response in the past (60, 61), suggesting that the improved elimusertib response in the PDX may in part be due to the *de novo BRCA1* mutation. Furthermore, ERMS_2b

acquired a mutation in *SETD2* during SoC treatment, which has been shown to enhance sensitivity to ATR inhibition in other tumor entities (30). In addition, we examined two Ewing sarcoma PDX derived from the same patient (EWS_3a+b). The first model (EWS_3a) was established at diagnosis, whereas the second PDX (EWS_3b) was established from the same patient after neo-adjuvant chemotherapy. Strikingly, the second sample responded better to elimusertib (Fig. 6C; Supplementary Fig. S5N and S5O), indicating that changes during neo-adjuvant chemotherapy may have enhanced susceptibility to elimusertib. Interestingly, many focal oncogene amplifications (e.g., *MYC*, *CCND1*, *MYCN*, and *MDM2*) were detectable in EWS_3b but not EWS_3a (Fig. 6C). In line with previous reports (27, 28) and our *in vitro* data (Fig. 1M), *MYCN* was one of the oncogenes mostly amplified in the responsive PDX (Fig. 6A and C). Gene amplifications can arise as a result of genomic instability and can occur in linear or extrachromosomal form (i.e., ecDNA). This raises the possibility that genomic instability and/or the type of gene amplification may influence ATR inhibitor sensitivity.

Discussion

Through an in-depth preclinical assessment of elimusertib's antitumor activity in a broad spectrum of patient-derived pediatric solid tumor models *in vitro* and *in vivo*, we here demonstrate that pharmacological ATR inhibition represents a therapeutic strategy with high clinical potential.

We and others have previously shown that diverse ATR inhibitors exhibit preclinical activity against a subset of ARMS, rhabdoid tumors, osteosarcoma, Ewing sarcoma, *MYCN*-amplified neuroblastomas and medulloblastomas (24–26, 28, 29, 62), but most of these studies only tested a small number of preclinical models and used ATR inhibitors that are currently not being clinically developed for the use in pediatric

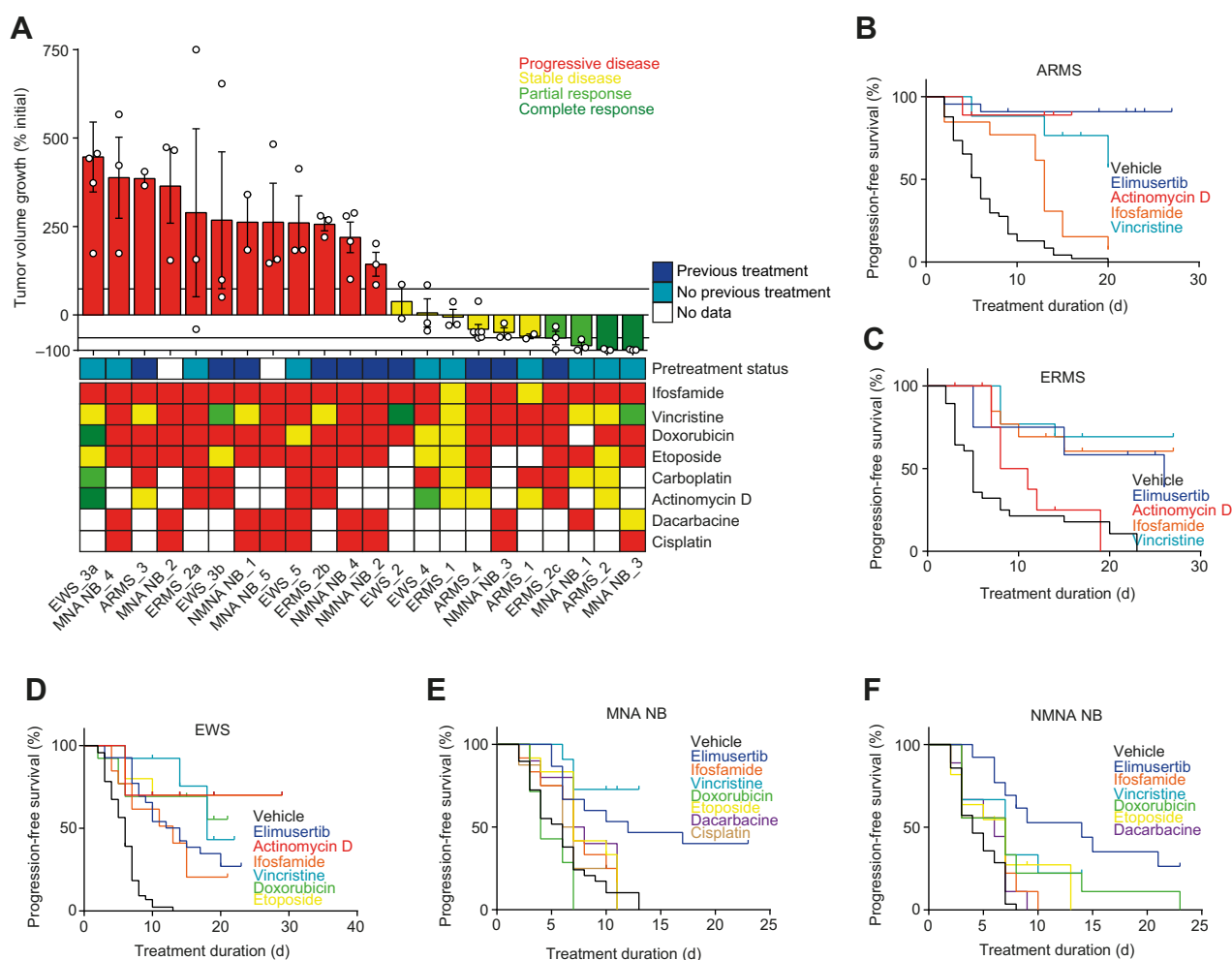


Figure 5. Elimusertib treatment shows that a progression-free survival benefit in a subset of preclinical pediatric solid tumors models compared with SoC treatment. **A**, Representation of the tumor volume after elimusertib treatment (top) and response to commonly used chemotherapeutic agents in our cohort of PDX models according to the RECIST criteria in a heat map (bottom, progressive disease, red; stable disease, yellow; partial response, light green; complete response, dark green;). In dark blue, PDX derived from patients that previously received SoC treatment are marked. **B–F**, Kaplan-Meier curves comparing the response of tumors with elimusertib, vehicle control treatment, or treatment with standard-of-care chemotherapeutic agents for ARMS (**B**, $n_{total} = 110$, $P < 0.0001$), ERMS (**C**, $n_{total} = 79$, $P < 0.0001$), Ewing sarcoma (**D**, $n_{total} = 132$, $P < 0.0001$), MNA NB (**E**, $n_{total} = 104$, $P < 0.0001$), and NMNA NB (**F**, $n_{total} = 88$, $P = 0.0003$). Log-rank tests were performed for statistical comparison. Single comparisons between elimusertib/SoC and vehicle treatment can be found in Supplementary Table S7.

patients. In line with our results, the antitumor activity of different clinical-stage ATR inhibitors as monotherapy and in combination with other agents has been widely recognized in cancers in adults (21, 22, 26, 39, 49, 60, 63–65).

In contrast with most ATR inhibitors, elimusertib is still in clinical development both for adult and pediatric patients (NCT04095273, NCT04616534, NCT04514497, and NCT05071209). Elimusertib's activity in most pediatric tumor entities, however, has not been assessed comprehensively to date. In an attempt to fill this gap of knowledge, we here performed a preclinical trial using state-of-the-art preclinical PDXs and broad molecular characterizations, similar to those performed by research consortia like the Pediatric Preclinical Testing Consortium. Compared with previous studies examining the antitumor activity ATR inhibitors in small numbers of *in vivo* models, our study provides insights on the inter-tumor response heterogeneity. The response heterogeneity observed in our study mirrors that of many

clinical trials for small molecules, suggesting that preclinical trials of this scale may predict clinical responses more closely than preclinical testing using low number of *in vivo* models. High costs of preclinical trials at this scale remain one of the main limitations of such studies. However, we propose that preclinical trials at similar scale as the one performed here should be considered as a standard for preclinical assessments in pediatric oncology.

Previous preclinical trials for various therapeutic interventions conventionally did not compare the effects of the tested intervention to SoC drugs. In fact, very little preclinical data exist for the antitumor efficacy of SoC drugs in preclinical patient-derived pediatric tumor models. This is mainly due to the fact that such models were not available to the same extent at the time SoC drugs were first selected for clinical testing. This raises several important questions. Even though many of the same SoC drugs are now considered the clinical gold standard for the treatment of different pediatric patients suffering from

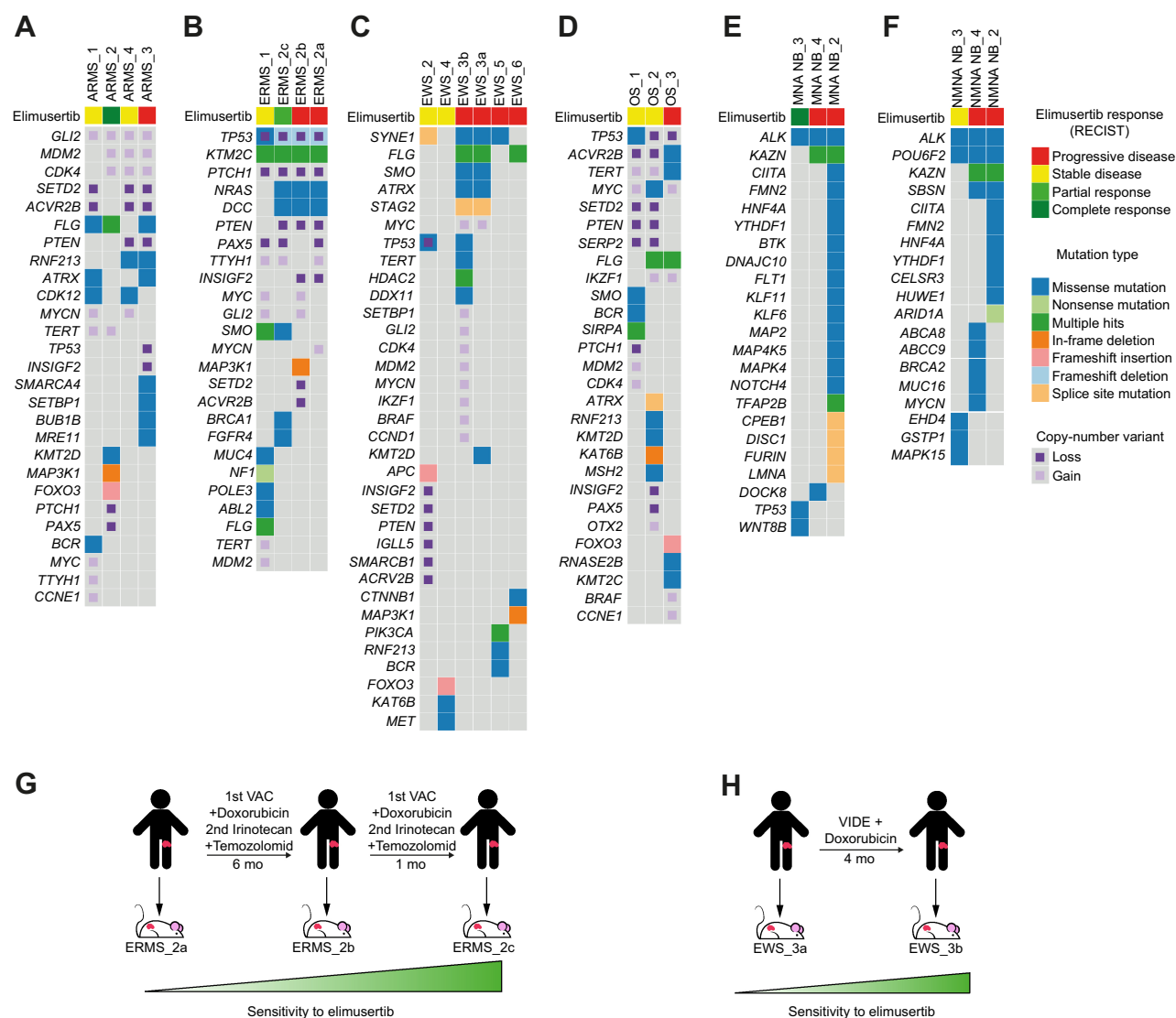


Figure 6. Genomic tumor evolution reveals mutations that are associated with altered response to elimusertib. **A–F**, Oncoplot showing mutations and CNVs present in PDX models for ARMS (**A**), ERMS (**B**), Ewing sarcoma (**C**), osteosarcoma (**D**), MNA NB (**E**), and NMNA NB (**F**). **G**, Timeline and chemotherapy treatment of a patient with ERMS and tumor response to elimusertib of the corresponding PDXs. The first PDX was established from a primary tumor. The patient received a cycle of vincristine, actinomycin D, and cyclophosphamide (VAC) complemented with low dosage of doxorubicin. A second line of treatment with irinotecan and temozolomide was added later on. Six months after the first biopsy, a biopsy from a relapsed tumor was used to establish a second PDX, and a new relapse after one month was used for the third PDX. **H**, Timeline and chemotherapy treatment of a patient with Ewing sarcoma and tumor response to elimusertib of the corresponding PDXs. The first PDX was established from a tumor biopsy used for diagnosis. The patient received a cycle of vincristine, ifosfamide, doxorubicin, and etoposide (VIDE) complemented with low dosage of doxorubicin. Four months after the initial biopsy, a biopsy from a relapsed tumor was used to establish a second PDX.

molecularly diverse tumor entities, we currently do not know how these SoC drugs perform preclinically. This lack of a true benchmark in preclinical trials creates problems when evaluating the efficacy of new treatment modalities. What antitumor effect should we consider as a positive result without such a benchmark? Do we currently set the bar too low or too high for new treatment modalities to be considered successful preclinically? To address these important limitations, we here compared the antitumor activity of elimusertib with that of SoC monotherapy in the same PDX models. This revealed that some SoC drugs perform surprisingly poor in many PDX when assessing response using clinically relevant read outs and raises the question

whether the same drugs would pass the threshold to be approved for clinical testing nowadays. We here compared the response with SoC drugs to that of elimusertib, a small-molecule inhibitor that very recently entered clinical testing in pediatric patients (NCT05071209). Notably, we observe that elimusertib showed a comparable and in some entities even a superior antitumor effect than SoC agents, particularly in ARMS. This is in line with our previous reports describing the exquisite sensitivity of ARMS cells to ATR inhibition, which at least in part seem due to PAX3–FOXO1-induced replication stress (29). We propose that based on both our previous and current studies on ATR inhibitors, patients suffering from ARMS should be

designated as a high-priority patient group in which ATR inhibitors should be tested clinically.

Biomarkers predicting clinical response to DDR inhibitors, including ATR inhibitors are still scarce. One of the most widely used molecular response predictor used for ATR inhibitors is ATM deficiency (22). Although we cannot exclude that ATM was epigenetically or otherwise compromised, we did not observe an association between the molecular ATM status and sensitivity of PDX models to elimusertib (Fig. 6A–F). Our findings stand in line with current clinical trial data showing that a large fraction of patients with ATM deficiency does not respond to ATR inhibitors (35). This suggests that other factors contribute to ATR inhibitor sensitivity. MYCN has been proposed to induce replication stress and sensitize cells to ATR inhibition (26). In line with these reports, MYCN-amplified neuroblastoma PDXs were among the most sensitive to elimusertib. We previously demonstrated that PAX3–FOXO1 expression can sensitize cells to ATR inhibition independent of MYCN expression (29). This raised the question whether gene amplification or the type of amplification rather than high oncogene expression may affect ATR inhibitor response. In line with our previous reports, PDX derived from ARMS expressing PAX3–FOXO1, were the most sensitive to elimusertib. Others have reported that fusion oncogene expression in general can sensitize cells ATR inhibition (25, 46). In our preclinical trial, however, neither EWS–FLI1-expressing Ewing sarcoma PDX nor CIC–DUX-expressing undifferentiated sarcoma PDX models responded particularly well to elimusertib. The lack of additional CIC–DUX-expressing undifferentiated sarcoma models limits definitive conclusions on the responsiveness of these tumors to elimusertib. As for Ewing sarcoma, we included 8 PDX models in our preclinical trial, 5 of which progressed during elimusertib treatment. This is in stark contrast with the reported sensitivity of Ewing sarcoma cells to ATR inhibition (25, 46). We cannot exclude, however, that the previously observed exceptional sensitivity of Ewing sarcoma was specific to the ATR inhibitors tested in these studies and that the chemical or pharmacologic properties of elimusertib influence its activity on Ewing sarcoma cells. Thus, we here provide evidence that ARMS and MYCN-amplified neuroblastomas are most sensitive to elimusertib both *in vitro* and *in vivo*, suggesting that patients suffering from these tumor entities may profit from elimusertib treatment.

In summary, elimusertib is active against preclinical patient-derived pediatric solid tumor models. These data support the initiation of clinical trials with elimusertib in patients with MYCN-amplified neuroblastomas and ARMS, and also provide evidence that some tumor entities may not respond as well to elimusertib as previously expected.

Authors' Disclosures

F.F. Pusch reports grants from Deutsche Forschungsgemeinschaft (DFG, German Research Foundation), Wilhelm Sander Stiftung, Charite; 3 R, Charite–Universitätsmedizin Berlin, and German Cancer Consortium (DKTK), as well as reports other support from BIH–Charite; Clinical Scientist Program funded by Charite–Universitätsmedizin Berlin, and personal fees and other support from Bayer AG, and grants from European Research Council (ERC) under the European Union's Horizon 2020 research and innovation program (grant agreement No. 949172), as well as reports other support from Deutsche Krebshilfe (German Cancer Aid) Mildred–Scheel Professorship program and NIH/CRUK (398299703, the eDynamic Cancer Grand Challenge), and grants and other support from la Caixa foundation (LCF/BQ/EU18/11650037) during the conduct of the study; other support from Bayer AG, personal fees from Bayer AG, and

other support from Eonic Biosciences outside the submitted work. A. Eggert reports personal fees from Recordati outside the submitted work. M.V. Ortiz reports grants from Amgen and personal fees from Guidepoint Global outside the submitted work. A.M. Wengner reports personal fees from Commercial sponsor outside the submitted work; and reports employment with Bayer AG. A.G. Henssen reports grants from Bayer during the conduct of the study; as well as reports personal fees from Eonic Biosciences outside the submitted work. No disclosures were reported by the other authors.

Authors' Contributions

F.F. Pusch: Conceptualization, resources, data curation, software, formal analysis, supervision, funding acquisition, validation, investigation, visualization, methodology, writing–original draft, project administration, writing–review and editing, co-first authorship. **H. Dorado Garcia:** conceptualization, resources, data curation, software, formal analysis, supervision, funding acquisition, validation, investigation, visualization, methodology, writing–original draft, project administration, writing–review and editing, co-first authorship. **R. Xu:** Resources, data curation, software, validation, investigation, visualization, writing–original draft, writing–review and editing. **D. Gürgen:** Conceptualization, resources, investigation, methodology. **Y. Bei:** Conceptualization, investigation, methodology. **L. Brückner:** Data curation, writing–original draft, writing–review and editing. **C. Röefzaad:** Resources, validation, investigation, writing–original draft. **J. von Stebut:** Supervision, validation, investigation. **V. Bardinet:** Validation, investigation, visualization, methodology. **R. Chamorro Gonzalez:** Data curation, writing–original draft, writing–review and editing. **A. Eggert:** Conceptualization, writing–original draft, writing–review and editing. **J.H. Schulte:** Conceptualization, writing–original draft, writing–review and editing. **P. Hundsdörfer:** Conceptualization, writing–original draft, writing–review and editing. **G. Seifert:** Conceptualization, writing–original draft, writing–review and editing. **K. Haase:** Software, formal analysis, validation, investigation, methodology, writing–review and editing. **B.W. Schäfer:** Resources, writing–review and editing. **M. Wachtel:** Resources, writing–review and editing. **A.A. Kühhl:** Resources, validation, investigation, visualization, methodology, writing–original draft, writing–review and editing. **M.V. Ortiz:** Conceptualization, supervision, writing–original draft, writing–review and editing. **A.M. Wengner:** Resources, supervision, funding acquisition, writing–review and editing. **M. Scheer:** Conceptualization, supervision, methodology, writing–original draft, writing–review and editing. **A.G. Henssen:** Conceptualization, resources, data curation, supervision, funding acquisition, validation, methodology, writing–original draft, project administration, writing–review and editing.

Acknowledgments

We would like to express our gratitude to the patients and families for providing tumor samples to the PDX BioBank of Charite – Universitätsmedizin Berlin. We thank Experimental Pharmacology and Oncology GmbH and iPATH.Berlin for their technical support. We want to thank Bayer for providing elimusertib and their financial support for conducting preclinical studies using that drug. H. Dorado Garcia received a fellowship (code LCF/BQ/EU18/11650037) from “la Caixa” Foundation (ID 100010434). A.G. Henssen is supported by the Deutsche Forschungsgemeinschaft (DFG, German Research Foundation) – 398299703 and the Wilhelm Sander Stiftung. This project has received funding from the European Research Council (ERC) under the European Union's Horizon 2020 research and innovation program (grant agreement No. 949172; to A.G. Henssen and H. Dorado Garcia). This research was financially supported by the Charité 3R, Charité–Universitätsmedizin Berlin (to A.G. Henssen). A.G. Henssen is supported by the German Cancer Consortium (DKTK). A.G. Henssen is a participant in the BIH–Charité Clinical Scientist Program funded by the Charité – Universitätsmedizin Berlin and the Berlin Institute of Health. This work was supported by the Deutsche Krebshilfe (German Cancer Aid) – 70114107 (Mildred–Scheel Professorship), 70113870 and 70113871 (to A.G. Henssen).

Note

Supplementary data for this article are available at Molecular Cancer Therapeutics Online (<http://mct.aacrjournals.org/>).

Received February 13, 2023; revised September 12, 2023; accepted December 26, 2023; published first December 29, 2023.

References

- Steliarova-Foucher E, Colombet M, Ries LAG, Moreno F, Dolya A, Bray F, et al. International incidence of childhood cancer, 2001–10: a population-based registry study. *Lancet Oncol* 2017;18:719–31.
- Siegel RL, Miller KD, Fuchs HE, Jemal A. Cancer statistics, 2022. *CA Cancer J Clin* 2022;72:7–33.
- Suh E, Stratton KL, Leisenring WM, Nathan PC, Ford JS, Freyer DR, et al. Late mortality and chronic health conditions in long-term survivors of early-adolescent and young adult cancers: a retrospective cohort analysis from the childhood cancer survivor study. *Lancet Oncol* 2020;21:421–35.
- Ma X, Liu Y, Alexandrov LB, Edmonson MN, Gawad C, Zhou X, et al. Pan-cancer genome and transcriptome analyses of 1,699 paediatric leukaemias and solid tumours. *Nature* 2018;555:371–6.
- Anderson ND, de Borja R, Young MD, Fuligni F, Rosic A, Roberts ND, et al. Rearrangement bursts generate canonical gene fusions in bone and soft tissue tumors. *Science* 2018;361:eaam8419.
- Brodeur GM, Seeger RC, Schwab M, Varmus HE, Bishop JM. Amplification of N-myc in untreated human neuroblastomas correlates with advanced disease stage. *Science* 1984;224:1121–4.
- Schwab M, Ellison J, Busch M, Rosenau W, Varmus HE, Bishop JM. Enhanced expression of the human gene N-myc consequent to amplification of DNA may contribute to malignant progression of neuroblastoma. *Proc Natl Acad Sci USA* 1984;81:4940–4.
- Kim H, Nguyen NP, Turner K, Wu S, Gujar AD, Luebeck J, et al. Extrachromosomal DNA is associated with oncogene amplification and poor outcome across multiple cancers. *Nat Genet* 2020;52:891–7.
- van Leen E, Bruckner L, Henssen AG. The genomic and spatial mobility of extrachromosomal DNA and its implications for cancer therapy. *Nat Genet* 2022;54:107–14.
- Yi E, Chamorro Gonzalez R, Henssen AG, Verhaak RGW. Extrachromosomal DNA amplifications in cancer. *Nat Rev Genet* 2022;23:760–71.
- Hanahan D, Weinberg RA. Hallmarks of cancer: the next generation. *Cell* 2011;144:646–74.
- Cheng B, Pan W, Xing Y, Xiao Y, Chen J, Xu Z. Recent advances in DDR (DNA damage response) inhibitors for cancer therapy. *Eur J Med Chem* 2022;230:114109.
- Gorgoulis VG, Vassiliou LV, Karakaidos P, Zacharatos P, Kotsinas A, Liloglou T, et al. Activation of the DNA damage checkpoint and genomic instability in human precancerous lesions. *Nature* 2005;434:907–13.
- Di Micco R, Fumagalli M, Cicalese A, Piccinin S, Gasparini P, Luise C, et al. Oncogene-induced senescence is a DNA damage response triggered by DNA hyper-replication. *Nature* 2006;444:638–42.
- Halazonetis TD, Gorgoulis VG, Bartek J. An oncogene-induced DNA damage model for cancer development. *Science* 2008;319:1352–5.
- Jackson SP, Bartek J. The DNA-damage response in human biology and disease. *Nature* 2009;461:1071–8.
- Blackford AN, Jackson SP. ATM, ATR, and DNA-PK: the trinity at the heart of the DNA damage response. *Mol Cell* 2017;66:801–17.
- Cimprich KA, Cortez D. ATR: an essential regulator of genome integrity. *Nat Rev Mol Cell Biol* 2008;9:616–27.
- Zeman MK, Cimprich KA. Causes and consequences of replication stress. *Nat Cell Biol* 2014;16:2–9.
- López-Contreras AJ, Gutierrez-Martinez P, Specks J, Rodrigo-Perez S, Fernandez-Capetillo O. An extra allele of Chk1 limits oncogene-induced replicative stress and promotes transformation. *J Exp Med* 2012;209:455–61.
- Gilad O, Nabet BY, Ragland RL, Schoppy DW, Smith KD, Durham AC, et al. Combining ATR suppression with oncogenic Ras synergistically increases genomic instability, causing synthetic lethality or tumorigenesis in a dosage-dependent manner. *Cancer Res* 2010;70:9693–702.
- Reaper PM, Griffiths MR, Long JM, Charrier JD, Maccormick S, Charlton PA, et al. Selective killing of ATM- or p53-deficient cancer cells through inhibition of ATR. *Nat Chem Biol* 2011;7:428–30.
- Kok YP, Guerrero Llobet S, Schoonen PM, Everts M, Bhattacharya A, Fehrmann RSN, et al. Overexpression of cyclin E1 or Cdc25A leads to replication stress, mitotic aberrancies, and increased sensitivity to replication checkpoint inhibitors. *Oncogenesis* 2020;9:88.
- Henssen AG, Reed C, Jiang E, Garcia HD, von Stebut J, MacArthur IC, et al. Therapeutic targeting of PGBD5-induced DNA repair dependency in pediatric solid tumors. *Sci Transl Med* 2017;9:eaam9078.
- Nieto-Soler M, Morgado-Palacin I, Lafarga V, Lecona E, Murga M, Callen E, et al. Efficacy of ATR inhibitors as single agents in Ewing sarcoma. *Oncotarget* 2016;7:58759–67.
- Roeschert I, Poon E, Henssen AG, Garcia HD, Gatti M, Giansanti C, et al. Combined inhibition of Aurora-A and ATR kinase results in regression of MYCN-amplified neuroblastoma. *Nat Cancer* 2021;2:312–26.
- Murga M, Campaner S, Lopez-Contreras AJ, Toledo LJ, Soria R, Montana MF, et al. Exploiting oncogene-induced replicative stress for the selective killing of Myc-driven tumors. *Nat Struct Mol Biol* 2011;18:1331–5.
- King D, Southgate HED, Roetschke S, Gravells P, Fields L, Watson JB, et al. Increased replication stress determines ATR inhibitor sensitivity in neuroblastoma cells. *Cancers* 2021;13:6215.
- Dorado Garcia H, Pusch F, Bei Y, von Stebut J, Ibanez G, Guillan K, et al. Therapeutic targeting of ATR in alveolar rhabdomyosarcoma. *Nat Commun* 2022;13:4297.
- Zimmermann M, Bernier C, Kaiser B, Fournier S, Li L, Desjardins J, et al. Guiding ATR and PARP inhibitor combinations with chemogenomic screens. *Cell Rep* 2022;40:111081.
- Wengner AM, Siemeister G, Lücking U, Lefranc J, Wortmann L, Lienau P, et al. The novel ATR inhibitor BAY 1895344 is efficacious as monotherapy and combined with DNA damage-inducing or repair-compromising therapies in preclinical cancer models. *Mol Cancer Ther* 2020;19:26–38.
- Lücking U, Wortmann L, Wengner AM, Lefranc J, Lienau P, Briem H, et al. Damage incorporated: discovery of the potent, highly selective, orally available ATR inhibitor BAY 1895344 with favorable pharmacokinetic properties and promising efficacy in monotherapy and in combination treatments in preclinical tumor models. *J Med Chem* 2020;63:7293–325.
- Gatz SA, Shipley J, Keller C, Linardic CM. Experimental Models. In: Arndt CAS, editor. *Sarcomas of Bone and Soft Tissues in Children and Adolescents*. Cham, Switzerland: Springer; 2021. p. 129–48.
- Timme N, Han Y, Liu S, Yosief HO, Garcia HD, Bei Y, et al. Small-molecule dual PLK1 and BRD4 inhibitors are active against preclinical models of pediatric solid tumors. *Transl Oncol* 2020;13:221–32.
- Yap TA, Tan DSP, Terbuch A, Caldwell R, Guo C, Goh BC, et al. First-in-Human trial of the oral ataxia telangiectasia and RAD3-related (ATR) inhibitor BAY 1895344 in patients with advanced solid tumors. *Cancer Discov* 2021;11:80–91.
- Casper AM, Nghiem P, Arlt MF, Glover TW. ATR regulates fragile site stability. *Cell* 2002;111:779–89.
- McNees CJ, Tejera AM, Martínez P, Murga M, Mulero F, Fernandez-Capetillo O, et al. ATR suppresses telomere fragility and recombination but is dispensable for elongation of short telomeres by telomerase. *J Cell Biol* 2010;188:639–52.
- Kalsbeek D, Golsteyn RM. G₂-M-phase checkpoint adaptation and micronuclei formation as mechanisms that contribute to genomic instability in human cells. *Int J Mol Sci* 2017;18:2344.
- Szydzik J, Lind DE, Arefin B, Kurhe Y, Umaphathy G, Siaw JT, et al. ATR inhibition enables complete tumour regression in ALK-driven NB mouse models. *Nat Commun* 2021;12:6813.
- Liu Q, Guntuku S, Cui XS, Matsuoka S, Cortez D, Tamai K, et al. Chk1 is an essential kinase that is regulated by Atr and required for the G(2)/M DNA damage checkpoint. *Genes Dev* 2000;14:1448–59.
- Busino L, Chiesa M, Draetta GF, Donzelli M. Cdc25A phosphatase: combinatorial phosphorylation, ubiquitylation, and proteolysis. *Oncogene* 2004;23:2050–6.
- Smith J, Tho LM, Xu N, Gillespie DA. The ATM-Chk2 and ATR-Chk1 pathways in DNA damage signaling and cancer. *Adv Cancer Res* 2010;108:73–112.
- Prigent C, Dimitrov S. Phosphorylation of serine 10 in histone H3, what for? *J Cell Sci* 2003;116:3677–85.
- Santos-Pereira JM, Aguilera A. R loops: new modulators of genome dynamics and function. *Nat Rev Genet* 2015;16:583–97.
- Boros-Olah B, Dobos N, Hornyak L, Szabo Z, Karanyi Z, Halmos G, et al. Drugging the R-loop interactome: RNA–DNA hybrid binding proteins as targets for cancer therapy. *DNA Repair* 2019;84:102642.
- Gorghi A, Romero JC, Loranc E, Cao L, Lawrence LA, Goodale E, et al. EWS–FLI1 increases transcription to cause R-loops and block BRCA1 repair in Ewing sarcoma. *Nature* 2018;555:387–91.
- Gröbner SN, Worst BC, Weischenfeldt J, Buchhalter I, Kleinheinz K, Rudneva VA, et al. The landscape of genomic alterations across childhood cancers. *Nature* 2018;555:321–7.

48. Hustedt N, Álvarez-Quilón A, McEwan A, Yuan JY, Cho T, Koob L, et al. A consensus set of genetic vulnerabilities to ATR inhibition. *Open Biol* 2019;9:190156.
49. Williamson CT, Miller R, Pemberton HN, Jones SE, Campbell J, Konde A, et al. ATR inhibitors as a synthetic lethal therapy for tumours deficient in ARID1A. *Nat Commun* 2016;7:13837.
50. DepMap, Broad (2021): DepMap 21Q2 Public. figshare. Dataset. Available from: <https://doi.org/10.6084/m9.figshare.14541774.v2>.
51. Koche RP, Rodriguez-Fos E, Helmsauer K, Burkert M, MacArthur IC, Maag J, et al. Extrachromosomal circular DNA drives oncogenic genome remodeling in neuroblastoma. *Nat Genet* 2020;52:29–34.
52. Helmsauer K, Valieva ME, Ali S, Chamorro Gonzalez R, Schopflin R, Roefzaad C, et al. Enhancer hijacking determines extrachromosomal circular MYCN amplification architecture in neuroblastoma. *Nat Commun* 2020;11:5823.
53. Manzella G, Schreck LD, Breunis WB, Molenaar J, Merks H, Barr FG, et al. Phenotypic profiling with a living biobank of primary rhabdomyosarcoma unravels disease heterogeneity and AKT sensitivity. *Nat Commun* 2020;11:4629.
54. Eisenhauer EA, Therasse P, Bogaerts J, Schwartz LH, Sargent D, Ford R, et al. New response evaluation criteria in solid tumours: revised RECIST guideline (version 1.1). *Eur J Cancer* 2009;45:228–47.
55. Schiavon G, Ruggiero A, Schöffski P, van der Holt B, Bekers DJ, Eechoute K, et al. Tumor volume as an alternative response measurement for imatinib-treated GIST patients. *PLoS ONE* 2012;7:e48372.
56. Chen C, Dorado Garcia H, Scheer M, Henssen AG. Current and future treatment strategies for rhabdomyosarcoma. *Front Oncol* 2019;9:1458.
57. Gill J, Gorlick R. Advancing therapy for osteosarcoma. *Nat Rev Clin Oncol* 2021;18:609–24.
58. Zollner SK, Amatruda JF, Bauer S, Collaud S, de Alava E, DuBois SG, et al. Ewing sarcoma—diagnosis, treatment, clinical challenges, and future perspectives. *J Clin Med* 2021;10:1685.
59. Moreno L, Barone G, DuBois SG, Molenaar J, Fischer M, Schulte J, et al. Accelerating drug development for neuroblastoma: summary of the second neuroblastoma drug development strategy forum from innovative therapies for children with cancer and international society of paediatric oncology Europe neuroblastoma. *Eur J Cancer* 2020;136:52–68.
60. Kim H, George E, Ragland R, Rafail S, Zhang R, Krepler C, et al. Targeting the ATR/CHK1 Axis with PARP inhibition results in tumor regression in *BRCA*-mutant ovarian cancer models. *Clin Cancer Res* 2017;23:3097–108.
61. Yazinski SA, Comaills V, Buisson R, Genoie MM, Nguyen HD, Ho CK, et al. ATR inhibition disrupts rewired homologous recombination and fork protection pathways in PARP inhibitor-resistant *BRCA*-deficient cancer cells. *Genes Dev* 2017;31:318–32.
62. Li X, Dean DC, Cote GM, Zou L, Hornicek FJ, Yu S, et al. Inhibition of ATR–Chk1 signaling blocks DNA double-strand-break repair and induces cytoplasmic vacuolization in metastatic osteosarcoma. *Ther Adv Med Oncol* 2020;12:1758835920956900.
63. Kwok M, Davies N, Agathangelou A, Smith E, Oldreive C, Petermann E, et al. ATR inhibition induces synthetic lethality and overcomes chemoresistance in TP53- or ATM-defective chronic lymphocytic leukemia cells. *Blood* 2016;127:582–95.
64. Lloyd RL, Wijnhoven PWG, Ramos-Montoya A, Wilson Z, Illuzzi G, Falenta K, et al. Combined PARP and ATR inhibition potentiates genome instability and cell death in ATM-deficient cancer cells. *Oncogene* 2020;39:4869–83.
65. Jette NR, Radhamani S, Arthur G, Ye R, Goutam S, Bolyos A, et al. Combined poly-ADP ribose polymerase and ataxia-telangiectasia mutated/Rad3-related inhibition targets ataxia-telangiectasia mutated-deficient lung cancer cells. *Br J Cancer* 2019;121:600–10.